Neuropeptide oxytocin facilitates its own brain-to-periphery uptake by regulating blood flow dynamics and permeability

Preethi Rajamannar[1,2], Oren Raz[3] and Gil Levkowitz[1,2*]

Departments of [1]Molecular Cell Biology, [2]Molecular Neuroscience, and [3]Physics of Complex Systems, Weizmann Institute of Science, PO Box 26, Rehovot 7610001, Israel

*Correspondence should be addressed to

G.L. gil.levkowitz@weizmann.ac.il

Running title: Oxytocin regulates pituitary blood flow and permeability

Key words: neurohormones, oxytocin, arginine-vasopressin, neurohypophysis, neuroendocrine

Abstract

The hypothalamo-neurohypophyseal system is an important neuroendocrine brain-to-blood conduit through which the neurohormones oxytocin and arginine-vasopressin are released from the brain into the general circulation to affect peripheral physiological functions such as salt balance, metabolism and reproduction. However, whether an active mechanism executes fast and efficient neurohormone release to the periphery remains unsolved. We show that a hyperosmotic physiological challenge elicits a local increase in neurohypophyseal blood flow velocities and a change in capillary diameter, which is dictated by the geometry of the hypophyseal vascular microcircuit. Genetic ablation of oxytocin neurons and inhibition of oxytocin receptor signaling attenuated capillary blood flow and diameter. Optogenetic stimulation of oxytocin neurons resulted in an oxytocin receptor-dependent increase in blood flow velocities. Lastly, both osmotic challenge and oxytocin neuronal activation elicited a local rise in neurohypophyseal capillary permeability in an oxytocin signaling-dependent manner. Our study demonstrates that physiologically elicited changes in neurohypophyseal blood flow and permeability are regulated by oxytocin. We propose that oxytocin-dependent neuro-vascular coupling facilitates its efficient uptake into the blood circulation, suggesting a self-perpetuating mechanism of peripheral hormone transfer.

INTRODUCTION

How the brain exerts control over peripheral functions is a fundamental question that has occupied researchers for over a century. In the early 1900s, Berta and Ernest Scharrer noticed that neurons residing in the hypothalamus of a small freshwater fish have properties similar to hormone-secreting endocrine cells (*1, 2*). This discovery served as an inspiration for Scharrers' "neurosecretion concept", arguing that hypothalamic neurons release packets of neuro-hormones from the brain into the general circulation by directly projecting their axons onto local blood vessels of the posterior pituitary gland, also known as the neurohypophysis. This brain-to-periphery neurosecretion machinery termed the hypohalamo-neurohypophyseal system (HNS), is evolutionarily conserved among all vertebrate species and is a major neuroendocrine system responsible for the secretion of the neuro-hormones oxytocin (OXT) and arginine-vasopressin (AVP) from hypothalamic axonal termini onto fenestrated (i.e., permeable) capillary network of the neurohypophysis to affect peripheral organs. In the periphery, AVP regulates water homeostasis by increasing the water permeability of the kidney, whereas OXT regulates labor and milk let-down by causing the contraction of the uterine smooth muscles and the myoepithelial cells of breast ducts, respectively(*3, 4*). In teleost fish species, OXT and AVP are involved in osmoregulation and regulating reproductive success(*5, 6*).

Despite the physiological importance of OXT and AVP, there is a gap in our understanding of their regulated secretion into the blood. The prevailing dogma maintains that in response to physiological demands, hypothalamic OXT and/or AVP neurons are stimulated, released from the axonal termini into the neurohypophysis, taken up by blood capillaries into the systemic circulation, and transported to target tissues (*7*). This process requires tight regulation between the secretory neurons, the release of the hormones, and their transport into the blood. However, it has been noted that a simplified stimulus–secretion coupling mechanism, wherein the release of the contents of vesicles upon neuronal activation (e.g. neurotransmitter release), is directly associated with its effect on the target neuron does not apply in the context of neuroendocrine effect on peripheral targets (*8*). Thus, while the measured firing rhythms of OXT and/or AVP neurons range within milliseconds or even seconds, it takes several minutes to detect them in the peripheral blood (*9*). Moreover, unlike the dense synaptic connection between neurons or the tightly arranged neurovascular units observed in the brain, HNS nerve endings do not form compact, juxtaposed connections with pituitary blood vessels. They rather form numerous

axonal varicosities packed with large dense core vesicles that release their content into the neurohypophysis, wherein the secreted neurohormones are required to transverse the cell-abundant pituitary parenchyma, the endothelial basement membrane, and then enter the endothelial lumen (*10*). ***It is, therefore, highly plausible that an additional driving force is required to facilitate efficient coupling between neurohormone release and its vascular uptake, leading to downstream effects on peripheral target tissues.*** In the brain, synaptic activity increases local blood flow to meet the metabolic needs of a firing neuron, a process termed neurovascular coupling. It has been suggested that endocrine cells of the pituitary gland and pancreas are coordinated with blood vessels to generate hormone pulses (*11, 12*). Thus, local blood flow in neuroendocrine interfaces may facilitate efficient hormone uptake rather than just a means to cope with the increased demands for oxygen.

Here, we hypothesized that in the neurohypophysis, activity-dependent changes in local blood flow modulate peripheral neurohormone uptake. Using live imaging of the zebrafish HNS, we monitored hypophyseal vascular dynamics in unanesthetized animals. We demonstrate that the physiological activation of oxytocin neurons is directly coupled to changes in blood flow velocity and capillary permeability. We further demonstrate that these physiologically elicited vascular changes are regulated by oxytocin, suggesting that oxytocin facilitates its own brain-to-periphery effects.

RESULTS

Physiological osmotic challenge increases local neurohypophyseal blood flow

To study neuro-vascular coupling in the HNS, we have devised a live-imaging platform using the zebrafish model. We have previously established that the development, cell biology, and anatomy of the HNS neurovascular interface are conserved between zebrafish and mammals (*13-15*). The core components of larval zebrafish HNS neurovascular interface comprised of elaborate oxytocinergic axonal varicosities, the hypophyseal artery (HyA), which conveys blood flow into a capillary loop (HyC) and a venous hypophyseal outlet (HyV) (**Fig. 1A**). This relatively simple and discernible anatomical architecture allowed us to reproducibly monitor vascular dynamics in the same locale within multiple unanesthetized zebrafish larvae. To monitor blood flow, we employed the *Tg(l-fabp:DBP-EGFP)* reporter (*16, 17*) (**Fig. S1A**), in which a serum albumin-like molecule is labeled, allowing visualization and quantification

of flow velocities calculated from displacement time kymographs of red blood cells (RBC) (**Fig. S1B,C**). Capillary diameter was monitored using an endothelial-specific transgenic *Tg(kdrl:EGFP)* reporter (**Fig. S1D**).

To examine whether physiological activation of the HNS altered hypophyseal blood flow, we employed a hyperosmotic challenge, which is known to stimulate OXT and AVP neurons (*18, 19*) (**Fig. S1A'**). When zebrafish larvae were acutely transferred from freshwater to hyperosmotic solution equivalent to 50% seawater (17.5 ppt), we observed significant activation of OXT neurons, displaying increased *c-fos* expression in their soma (**Fig. 1B,C**). This hyperosmotic challenge induced a robust increase in blood flow (**Fig. 1D,E**) and variability of RBCs velocities (**Fig. 1F**). The single-sided amplitude spectra, as computed by a Fast Fourier transformation (FFT), indicated that the osmotic challenge induced an increase in the amplitude of velocity fluctuations below 2Hz (**Fig. 1G**).

To ensure that the effect of osmotic challenge on blood flow was specific to the hypophyseal capillary, we measured blood flow in the anterior mesencephalic central artery (AMCtA), which is a well-discernable vascular brain structure located at a similar depth and of similar diameter as the hypophyseal capillary loop (**Fig. 1A**). We found that osmotic challenge did not affect the measured flow parameters of AMCtA vessel (**Fig. 1H-K**).

These results show that a physiological challenge, which activates OXT neurons elicits a specific local increase in hypophyseal blood flow velocity.

The relationship between flow velocity and diameter is determined by HNS vascular geometry

According to Poiseuille's law for viscous fluids, it was expected that local vasoconstriction of a single capillary would increase flow resistance, resulting in decreased blood flow velocity (*20*). However, we observed that the osmotic challenge, which caused an increase in velocity was accompanied by a decrease in hypophyseal capillary diameter (**Fig. 2A-C**). This effect was specific as the diameter of the adjacent AMCtA capillary did not change following the osmotic challenge (**Fig. 2D-F**). Since it was shown that the geometry of the microvasculature network in the brain plays a crucial role in determining blood flow behaviour (*21, 22*), we resolved the relationship between blood flow velocity and capillary diameter considering the structure of

126 the zebrafish hypophyseal vascular microcircuit. This structure is comprised of a stereotypic
127 arterial inlet, capillary loop, and venous outlet; each having its corresponding resistance (R),
128 length (L), and radius (r) (**Fig. 2G**). We expressed the capillary velocity (V_2) in terms of the
129 vascular components' radii and lengths, according to Poiseuille's law, considering a range of
130 relevant inlet-outlet total pressure differences (Δp) (**Fig. 2G and S1E,** for details, see '*Methods*'
131 section). Plotting the resolved V_2 values as a function of capillary radii revealed that flow
132 velocity is inversely proportional to an increase in capillary radii that are larger than 3 microns
133 (**Fig. 2H**). This inverse proportionality between capillary velocity and diameter, aligned with
134 our measured values of the hypophyseal capillary radii (3-6 μm **Fig. 2B**). Thus, in accordance
135 with our velocity and radii measurements, we found that for basal velocity to increase after
136 osmotic challenge within a range of relevant estimated inlet-outlet pressure differences (Δp),
137 there must be either a small decrease in radii with a small increase in Δp or a large decrease in
138 radii with no change in Δp (**Fig. 2H'**).

139 These results show that an increase in blood flow velocity can be caused by vasoconstriction
140 given the geometry of the hypophyseal vascular microcircuit.

141

142 **Hypophyseal blood flow is regulated by oxytocin signaling**

143 We tested whether the observed neuronal and vascular responses to an osmotic challenge
144 are coupled. This was demonstrated using the *Tg(oxt:Gal4;UAS:NTR-mCherry)* genetic
145 system for conditional cell ablation (**Fig. 3A**). Specific death of OXT cells expressing the
146 nitroreductase (NTR) enzyme was induced by the administration of the drug Nifurpirinol
147 (NFP), which is converted to a cytotoxic agent by NTR (*23-25*). Treatment of these transgenic
148 animals for 18 hours with NFP led to a significant decrease in OXT-positive hypophyseal
149 axonal projections (**Fig. 3B,C**). When subjected to an osmotic challenge, control Gal4/UAS-
150 negative larvae displayed increased blood flow velocity while their sibling larvae with ablated
151 OXT neurons did not (**Fig. 3D,E**). The mean capillary blood flow velocity, amplitudes, and
152 frequency spectra, and variability in velocity did not show a significant difference after the
153 osmotic challenge of OXT ablated larvae (**Fig. 3F-I**). Notably, whereas the osmotic challenge
154 caused vasoconstriction in non-ablated controls, it led to vasodilation of hypophyseal
155 capillaries in larvae with ablated OXT neurons, presumably as a response to the absence of
156 OXT neurovascular innervation and low basal OXT secretion (**Fig. 3J-M**). The effects of this

genetic OXT-ergic ablation were confined to the hypophyseal vasculature as they were not observed in the control AMCtA vessel (**Fig. 3N-P**).

In view of our observed effects of OXT neuron ablation, we hypothesized that OXT itself might regulate local hypophyseal blood flow velocity upon its release. We found that endothelial cells isolated from zebrafish pituitaries express mRNAs encoding the two known functional OXT receptors, *oxtra,* and *oxtrb,* with markedly higher expression levels of *oxtrb* (**Fig. S2**). We therefore examined whether the administration of a selective oxytocin receptor antagonist, L-368,899, which is known to inhibit both zebrafish OXT receptors (*26, 27*), affects hypophyseal blood flow. We found that larvae treated with L-368, 899, were refractory to the osmotic challenge in terms of challenge-induced changes in mean flow velocity parameters (**Fig. 4A-F**) and capillary diameter (**Fig. 4G-J**). Administration of L-368, 899 did not influence blood flow velocity in the extra-hypophyseal AMCtA blood vessel ruling out a general systemic effect of the antagonist (**Fig. 4K-M**).

Next, we tested whether direct activation of OXT neurons, rather than through osmotic challenge, is sufficient to modulate hypophyseal blood flow and diameter. To stimulate OXT neurons, we employed the CoChR-tdTomato channelrhodopsin variant, an efficient optogenetic tool for zebrafish (*28*). Injection of *UAS:CoChR-tdTomato* construct into the OXT specific driver line, *Tg(oxt:Gal4)* (*29*), resulted in specific expression of the CoChR-tdTomato protein in OXT neurons (**Fig. 5A,B**). Exposure of *Tg(oxt:Gal4;UAS:CoChR-tdTomato)* larvae to blue light resulted in a transient but significant increase in blood flow velocity, which peaked at approximately 30-50 seconds following light exposure (**Fig. 5D,E**). The control CoChR-tdTomato-negative siblings did not respond to blue light (**Fig. 5C,E**). Light-activated CoChR-positive larvae exhibited a marked increase in $\Delta V/V_0$ as compared to their CoChR-negative siblings (**Fig. 5F**). The responses of hypophyseal vasculature to optogenetic stimulation of OXT neurons were dependent on oxytocin receptor signalling as the above effects were significantly attenuated by the administration of the OXT receptor antagonist, L-368, 899 (**Fig. 5G-I**). In accordance with the vasoconstrictive response of the hypophyseal capillary to osmotic challenge, light activation of CoChR-positive, but not CoChR-negative, OXT neurons caused a reduction in mean capillary diameter across time (**Fig. 5J-M**). As in the case of the increased flow velocity, CoChR-induced vasoconstrictive response was inhibited by L-368, 899 (**Fig. 5N-P**). Notably, hypophyseal vascular responses (i.e., flow and diameter) to optogenetic activation of OXT neurons were transient as compared to the hyperosmotic

189 challenge. Although this may imply the existence of additional mediators of the effects of
190 osmotic challenge on hypophyseal vascular dynamics, it could be due to the artificial activation
191 of OXT neurons through optogenetics, as opposed to a genuine physiological stimulus, which
192 activates these neurons.

193 These results show that local hypophyseal vascular responses triggered by a hyperosmotic
194 physiological challenge are coupled to OXT neuronal activation and are mediated by OXT
195 receptor(s).

196

197 **Hypophyseal vascular permeability is regulated by OXT signaling**

198 We hypothesized that OXT-mediated neurovascular-coupling may affect the vascular
199 passage of neurohormones and other proteins by regulating diffusion rate through the
200 fenestrated hypophyseal capillaries (*16*). We visualized and quantified hypophyseal capillary
201 permeability using the *Tg(l-fabp:DBP-EGFP)* reporter described above (**Fig. 6A**). We
202 performed fluorescent recovery after photo-bleaching (FRAP) followed by line scan imaging
203 comparing the fluorescent recovery of bleached and unbleached regions of interest positioned
204 on either side of the hypophyseal capillary (**Fig.6A',B**). Paired comparisons of permeability
205 before and after the challenge indicated that the average time taken to recover half the initial
206 fluorescent intensity ($T_{1/2}$) following an osmotic challenge was significantly shorter than in the
207 basal condition, indicating a higher rate of diffusion through the hypophyseal capillary (**Fig.**
208 **6C**).

209 We then investigated the inter-dependent relationship between blood flow velocity and
210 permeability. We have previously shown that Tgf-β signaling regulates hypophyseal vascular
211 permeability (*13*). We now show that albeit the observed attenuation of basal hypophyseal
212 permeability by the selective TGF-β receptor inhibitor, SB431542 (**Fig. 6D,E**), blocking Tgf-
213 β signaling did not affect either the basal blood flow velocity or the response to osmotic
214 challenge (**Fig. 6F**). We next examined whether decreasing blood flow affects permeability.
215 We observed that treatment of zebrafish larvae with the cholinergic receptor inhibitor alpha-
216 bungarotoxin (α-BTX) for 150 seconds led to a nearly 50% reduction in blood flow velocity
217 (**Fig. 6G-H**). This reduction in blood flow had no effect on hypophyseal vessel permeability
218 (**Fig. 6I**).

219 These results indicate that hypophyseal vascular permeability and blood flow velocity are
220 mutually independent.

221 To determine the involvement of OXT signaling in hypophyseal vascular permeability, we
222 performed the FRAP analysis in the presence of the OXT receptor antagonist. Basal
223 permeability was measured continuously at different time points following the administration
224 of the OXT receptor antagonist. A significant increase in $T_{1/2}$ was observed up to an hour after
225 the administration of the antagonist, indicating a cumulative decrease in protein diffusion rate
226 through the hypophyseal capillary (**Fig. 6J**). Furthermore, the permeability-enhancing effect
227 of OC was also attenuated in antagonist-treated larvae as compared to their untreated siblings
228 (**Fig. 6K**).

229 The involvement of OXT in modulating permeability was further determined by direct
230 optogenetic activation of OXT neurons combined with FRAP analysis. A significant decrease
231 in $T_{1/2}$ was measured in light-activated, CoChR-tdTomato-expressing larvae compared to their
232 inactivated basal state (**Fig. 6L**). The control CoChR-negative larvae showed no response to
233 light (**Fig. 6L**). Thus, direct activation of oxytocin neurons enhances hypophyseal
234 permeability.

235 Taken together, our data show that hyperosmotic physiological challenge elicits an increase
236 in local blood flow velocity and permeability of the hypophyseal vasculature, where OXT is
237 released into the peripheral circulation. These hypophyseal vascular responses are influenced
238 by the local vascular geometry and are coupled to OXT neuronal activation, which is mediated
239 by OXT receptors. We submit that OXT may function as a self-perpetuating hormone that
240 facilitates its own peripheral uptake by regulating blood flow dynamics.

241

242 **DISCUSSION**

243 Neurohormones are key factors interfacing between the brain and periphery, yet not much
244 is known about their behavior at the site of release, and in particular, the factors affecting their
245 uptake into the blood. We focus here on the evolutionarily conserved HNS, which is a canonical
246 neuroendocrine interface wherein neurohormones are directly released from the brain into the
247 blood. The data we have gathered indicates that when faced with a hyperosmotic physiological
248 challenge, there's a noticeable increase in hypophyseal blood flow velocity and vascular

permeability where OXT is released into the peripheral circulation. The local hypophyseal vascular responses to OXT neuronal activation are influenced by vascular geometry and mediated by OXT receptors. This leads us to propose that OXT may function as a self-perpetuating hormone, regulating its own peripheral uptake by influencing blood flow dynamics and permeability.

Neurovascular coupling in the HNS

Upon stimulation of OXT neurons, OXT is released from the nerve termini into the hypophyseal perivascular space and thereafter exerts effects on peripheral target tissues. However, there is a gap in our understanding of the exact events that bring about efficient transport of OXT to the periphery. Unlike the rapid, short-distanced post-synaptic actions of neurotransmitters in the brain, OXT must travel a long distance through the dense hypophyseal perivascular space and its concentration in the blood must increase rapidly in response to physiological demands. This suggests that additional factors may be required for an efficient coordination between the release of neurohormones and their peripheral effects. We hypothesized that activity-mediated axonal release needs to be coupled to blood flow to regulate an effective transfer of OXT into the systemic circulation. However, despite extensive understanding of the electrical activity of oxytocin (OXT) neurons, the role of local blood flow in coordinating neurohormone secretion remains unclear (*30, 31*). Lafont et al. inferred the existence of such a mechanism, demonstrating that the injection of growth hormone-releasing hormone (GHRH) leads to increased local blood flow, coinciding with the timing of the growth hormone (GH) pulse in the peripheral circulation (*32*). These authors discussed the possibility that flow dynamics of the pituitary microvasculature network may influence the pulsatile secretion of growth hormone (*32*).

We show here that an osmotic challenge stimulates OXT neuronal activity concomitant with a specific local increase in volumetric blood flow in the hypophyseal capillary abutting OXT axons termini. This result is in agreement with the reported increased neurohypophyseal blood flow in chronically water-deprived rats (*33, 34*). Others have recently shown a connection between osmotic challenge and changes in supraoptic nucleus (SON) blood flow (*35*). They reported that an acute systemic salt load activates AVP neurons, decreasing blood flow and causing temporary hypoxia, which intensifies the excitatory response of AVP neurons to the systemic hyperosmotic salt challenge (*35*).

280 Local regulation of organ perfusion rate relies on local changes in vascular resistance, which
281 is controlled by capillary radius (*36, 37*). Thus, local vasoconstriction of a single capillary,
282 obeying Poiseuille's flow, will increase resistance and decrease flow (*20*). Having said that, the
283 geometry of a particular microvasculature network, including factors such as capillary length,
284 branching patterns and positions of inlet-outlet, plays an important role in determining flow
285 velocity (*22, 38*). In the case of the specific configuration of the hypophyseal vascular circuit,
286 we found that blood flow velocity increases upon vasoconstriction. This result also fits our
287 theoretically resolved relationship between blood flow velocity and capillary diameter,
288 considering the specific architecture, lengths, and radii of the hypophyseal vascular
289 components.

290

291 **Role of oxytocin signaling**

292 Vascular endothelial cells were shown to express the OXT receptor and have been
293 implicated in the regulation of vascular tone and blood pressure in mammals and fish (*39-43*).
294 It was shown that OXT can exert both vasodilation and vasoconstriction via differential
295 activation of either endothelial nitric oxide or ERK signaling (*39*). We show here that, as in
296 other species, zebrafish OXT neurons are osmoresponsive, and the effect of osmotic challenge
297 on hypophyseal blood flow is mediated by OXT signaling. Similarly, increased osmolality,
298 which was induced by dehydration, led to an increased blood flow in the rat neurohypophysis
299 (*33, 34*). Using Brattleboro Kapitola et al. concluded that the increase in hypophyseal blood
300 flow following dehydration could not be mediated by AVP as these rats cannot synthesize this
301 neurohormone (*34*). However, it is likely that OXT is accountable for the observed dehydration
302 effect on rat hypophysis. This is supported by our findings that the impact of hyperosmotic
303 challenge is mediated by OXT signaling, and that direct optogenetic stimulation of OXT
304 neurons influences both blood flow and diameter.

305 We show that endothelial cells express OXT receptors and that blocking OXT signaling
306 attenuates the induced changes in blood flow and capillary diameter. However, it is important
307 to note that other cell types in the neurohypophysis may also play a role in OXT-mediated
308 vascular response. For example, pericytes have been implicated in the regulation of blood flow
309 in the brain (*44-46*). Additionally, hypophyseal astroglial pituicytes, which receive synaptoid

connections from HNS axon termini, facilitate the release of OXT and AVP to the periphery in response to parturition, lactation, and dehydration (*29, 47, 48*).

Hypophyseal vascular permeability

Although the HNS is considered part of the central nervous system, its vascular component has unique properties that differ from neurovascular units in other brain areas. Unlike most BBB-containing vessels of the CNS, neurohypophyseal capillaries are fenestrated, allowing bi-directional transfer of HNS hormones and blood-borne substances between the brain and circulation (*13, 16, 49*). Our research shows that protein diffusion through the hypophyseal capillary increases after a hyperosmotic challenge. Although we show that the increase in hypophyseal blood flow velocity and permeability appears to be independent of one other, both occur in an oxytocin-dependent manner. Thus, blocking OXT signaling decreases hypophyseal permeability and direct activation of OXT neurons enhances permeability.

Modulation of local blood flow has been linked to hormonal uptake in several instances. For example, somatostatin causes vasoconstriction, reducing blood flow and increasing vascular permeability of pial vessels of the parietal cortex (*50*). Blood flow in the median eminence, which contains fenestrated capillaries, influences food intake by regulating the access of ghrelin to the arcuate nucleus (*51, 52*). Finally, pericytes, which regulate blood flow (*45, 46*) were shown to regulate vascular permeability to circulating leptin (*53*). We propose that in the case of the neurohypophysis, oxytocin orchestrates an efficient neuroendocrine secretion machinery by affecting both hypophyseal blood flow velocity and permeability, thereby coupling its own release and transport into the blood.

Based on the results we have presented, we propose the following paradigm, which we term '***stimulus-secretion-uptake coupling***': When HNS neurons are stimulated, OXT is released into the hypophyseal parenchyma and establishes a concentration gradient of OXT between the parenchyma and the local capillary. The diffusion of OXT into the capillary tends to bring the system closer to equilibrium, thus reducing the diffusion of oxytocin into the vessel. The increase in local volumetric flow, which is induced by OXT, has a dual function: **1**) enhancing local transport of OXT to the periphery and **2**) increasing diffusion of the secreted OXT into the blood by maintaining a local oxytocin concentration gradient. This, together with the

increased permeability, which is also evoked by OXT, ensures its efficient transfer into the peripheral circulation in response to physiological demands.

REFERENCES

1. E. Scharrer, Die lichtempfindlichkeit blinder elritzen.(Untersuchungen über das zwischenhirn der fische I.). *Zeitschrift für vergleichende Physiologie*, (1928).
2. E. Scharrer, B. Scharrer, Neurosecretion. *Physiological Reviews* **25**, 171-181 (1945).
3. C. A. Pearson, M. Placzek, Development of the medial hypothalamus: forming a functional hypothalamic-neurohypophyseal interface. *Curr Top Dev Biol* **106**, 49-88 (2013).
4. E. Wircer, S. Ben-Dor, G. Levkowitz, in *Molecular neuroendocrinology : from genome to physiology*

, D. G. Murphy, Harold, Ed. (John Wiley & Sons, Ltd, Chichester, West Sussex, UK ; Hoboken, NJ, USA, 2016), pp. xiii, 467 pages.

5. J. Biran, J. Blechman, E. Wircer, G. Levkowitz, in *Model Animals in Neuroendocrinology: From Worm to Mouse to Man,* M. Ludwig, G. Levkowitz, Eds. (Wiley-Blackwell, 2018), pp. 101-103.
6. P. Rajamannar, I. Arokiadhas, G. Levkowitz, J. Biran, in *Neuroanatomy of Neuroendocrine Systems,* V. Grinevich, Á. Dobolyi, Eds. (Springer International Publishing, Cham, 2021), pp. 95-118.
7. G. Leng, M. Ludwig, Neurotransmitters and peptides: whispered secrets and public announcements. *J Physiol* **586**, 5625-5632 (2008).
8. P. Le Tissier *et al.*, An updated view of hypothalamic-vascular-pituitary unit function and plasticity. *Nat Rev Endocrinol* **13**, 257-267 (2017).
9. G. Leng, N. Sabatier, Measuring Oxytocin and Vasopressin: Bioassays, Immunoassays and Random Numbers. *J Neuroendocrinol* **28**, (2016).
10. G. I. Hatton, Pituicytes, glia and control of terminal secretion. *The Journal of experimental biology* **139**, 67-79 (1988).
11. M. Schaeffer, D. J. Hodson, C. Lafont, P. Mollard, Endocrine cells and blood vessels work in tandem to generate hormone pulses. *J Mol Endocrinol* **47**, R59-66 (2011).

12. M. Schaeffer, D. J. Hodson, C. Lafont, P. Mollard, Functional importance of blood flow dynamics and partial oxygen pressure in the anterior pituitary. *Eur J Neurosci* **32**, 2087-2095 (2010).
13. S. Anbalagan *et al.*, Pituicyte Cues Regulate the Development of Permeable Neuro-Vascular Interfaces. *Dev Cell* **47**, 711-726 e715 (2018).
14. A. Gutnick *et al.*, The hypothalamic neuropeptide oxytocin is required for formation of the neurovascular interface of the pituitary. *Dev. Cell* **21**, 642-654 (2011).
15. Q. Chen *et al.*, Neural plate progenitors give rise to both anterior and posterior pituitary cells. *Dev Cell* **58**, 2652-2665 e2656 (2023).
16. L. Gordon *et al.*, The fenestrae-associated protein Plvap regulates the rate of blood-borne protein passage into the hypophysis. *Development* **146**, (2019).
17. J. Xie, E. Farage, M. Sugimoto, B. Anand-Apte, A novel transgenic zebrafish model for blood-brain and blood-retinal barrier development. *BMC developmental biology* **10**, 76 (2010).
18. G. Leng, J. A. Russell, The osmoresponsiveness of oxytocin and vasopressin neurones: Mechanisms, allostasis and evolution. *J Neuroendocrinol* **31**, e12662 (2019).
19. I. Neumann, R. Landgraf, L. Bauce, Q. J. Pittman, Osmotic responsiveness and cross talk involving oxytocin, but not vasopressin or amino acids, between the supraoptic nuclei in virgin and lactating rats. *J Neurosci* **15**, 3408-3417 (1995).
20. S. P. Sutera, R. Skalak, The History of Poiseuille's Law. *Annual Review of Fluid Mechanics* **25**, 1-20 (1993).
21. P. Blinder *et al.*, The cortical angiome: an interconnected vascular network with noncolumnar patterns of blood flow. *Nat Neurosci* **16**, 889-897 (2013).
22. X. Ji *et al.*, Brain microvasculature has a common topology with local differences in geometry that match metabolic load. *Neuron* **109**, 1168-1187 e1113 (2021).
23. S. Curado, D. Y. Stainier, R. M. Anderson, Nitroreductase-mediated cell/tissue ablation in zebrafish: a spatially and temporally controlled ablation method with applications in developmental and regeneration studies. *Nat Protoc* **3**, 948-954 (2008).
24. D. Bergemann *et al.*, Nifurpirinol: A more potent and reliable substrate compared to metronidazole for nitroreductase-mediated cell ablations. *Wound Repair Regen* **26**, 238-244 (2018).
25. A. R. Nunes *et al.*, Developmental Effects of Oxytocin Neurons on Social Affiliation and Processing of Social Information. *J Neurosci* **41**, 8742-8760 (2021).

26. F. F. Zimmermann, K. V. Gaspary, A. M. Siebel, C. D. Bonan, Oxytocin reversed MK-801-induced social interaction and aggression deficits in zebrafish. *Behavioural Brain Research* **311**, 368-374 (2016).
27. J. Landin *et al.*, Oxytocin Receptors Regulate Social Preference in Zebrafish. *Sci Rep* **10**, 5435 (2020).
28. P. Antinucci *et al.*, A calibrated optogenetic toolbox of stable zebrafish opsin lines. *Elife* **9**, (2020).
29. S. Anbalagan *et al.*, Robo2 regulates synaptic oxytocin content by affecting actin dynamics. *Elife* **8**, (2019).
30. J. A. Russell, G. Leng, A. J. Douglas, The magnocellular oxytocin system, the fount of maternity: adaptations in pregnancy. *Front Neuroendocrinol* **24**, 27-61 (2003).
31. D. A. Poulain, J. B. Wakerley, Electrophysiology of hypothalamic magnocellular neurones secreting oxytocin and vasopressin. *Neuroscience* **7**, 773-808 (1982).
32. C. Lafont *et al.*, Cellular in vivo imaging reveals coordinated regulation of pituitary microcirculation and GH cell network function. *Proc Natl Acad Sci U S A* **107**, 4465-4470 (2010).
33. B. Lichardus, I. Albrecht, J. Ponec, L. Linhart, Water deprivation for 24 hours increases selectively blood flow in posterior pituitary of conscious rats. *Endocrinol Exp* **11**, 99-104 (1977).
34. J. Kapitola, H. Dlouha, J. Krecek, J. Zicha, The effect of dehydration on the neurohypophyseal blood flow in rats with hereditary diabetes insipidus. *Experientia* **33**, 1615-1616 (1977).
35. R. K. Roy *et al.*, Inverse neurovascular coupling contributes to positive feedback excitation of vasopressin neurons during a systemic homeostatic challenge. *Cell Rep* **37**, 109925 (2021).
36. A. R. Pries *et al.*, Resistance to blood flow in microvessels in vivo. *Circ Res* **75**, 904-915 (1994).
37. R. E. Shipley, D. E. Gregg, THE EFFECT OF EXTERNAL CONSTRICTION OF A BLOOD VESSEL ON BLOOD FLOW. *American Journal of Physiology-Legacy Content* **141**, 289-296 (1944).
38. P. Blinder, A. Y. Shih, C. Rafie, D. Kleinfeld, Topological basis for the robust distribution of blood to rodent neocortex. *Proc Natl Acad Sci U S A* **107**, 12670-12675 (2010).

436 39. Q. Xu *et al.*, Oxytocin-induced endothelial nitric oxide dependent vasorelaxation and
437 ERK1/2-mediated vasoconstriction in the rat aorta. *Korean J Physiol Pharmacol* **26**,
438 255-262 (2022).
439 40. N. Japundzic-Zigon, M. Lozic, O. Sarenac, D. Murphy, Vasopressin & Oxytocin in
440 Control of the Cardiovascular System: An Updated Review. *Curr Neuropharmacol* **18**,
441 14-33 (2020).
442 41. M. Petersson, T. Lundeberg, K. Uvnas-Moberg, Oxytocin decreases blood pressure in
443 male but not in female spontaneously hypertensive rats. *J Auton Nerv Syst* **66**, 15-18
444 (1997).
445 42. M. Jankowski, T. L. Broderick, J. Gutkowska, The Role of Oxytocin in Cardiovascular
446 Protection. *Front Psychol* **11**, 2139 (2020).
447 43. L. Haraldsen, V. Soderstrom-Lauritzsen, G. E. Nilsson, Oxytocin stimulates cerebral
448 blood flow in rainbow trout (Oncorhynchus mykiss) through a nitric oxide dependent
449 mechanism. *Brain Res* **929**, 10-14 (2002).
450 44. C. M. Peppiatt, C. Howarth, P. Mobbs, D. Attwell, Bidirectional control of CNS
451 capillary diameter by pericytes. *Nature* **443**, 700-704 (2006).
452 45. C. N. Hall *et al.*, Capillary pericytes regulate cerebral blood flow in health and disease.
453 *Nature* **508**, 55-60 (2014).
454 46. D. A. Hartmann *et al.*, Brain capillary pericytes exert a substantial but slow influence
455 on blood flow. *Nat Neurosci* **24**, 633-645 (2021).
456 47. L. Rosso, J. M. Mienville, Pituicyte modulation of neurohormone output. *Glia* **57**, 235-
457 243 (2009).
458 48. J. G. Tasker, S. H. Oliet, J. S. Bains, C. H. Brown, J. E. Stern, Glial regulation of
459 neuronal function: from synapse to systems physiology. *J Neuroendocrinol* **24**, 566-
460 576 (2012).
461 49. S. Miyata, New aspects in fenestrated capillary and tissue dynamics in the sensory
462 circumventricular organs of adult brains. *Front Neurosci* **9**, 390 (2015).
463 50. J. B. Long, D. D. Rigamonti, K. Dosaka, J. M. Kraimer, A. Martinez-Arizala,
464 Somatostatin causes vasoconstriction, reduces blood flow and increases vascular
465 permeability in the rat central nervous system. *J Pharmacol Exp Ther* **260**, 1425-1432
466 (1992).
467 51. N. Romano *et al.*, Median eminence blood flow influences food intake by regulating
468 ghrelin access to the metabolic brain. *JCI Insight* **8**, (2023).

52. M. Schaeffer *et al.*, Rapid sensing of circulating ghrelin by hypothalamic appetite-modifying neurons. *Proc. Natl. Acad. Sci. USA* **110**, 1512-1517 (2013).
53. L. I. Butiaeva *et al.*, Leptin receptor-expressing pericytes mediate access of hypothalamic feeding centers to circulating leptin. *Cell Metab* **33**, 1433-1448 e1435 (2021).
54. G. K. Batchelor, in *An introduction to fluid dynamics*. (Cambridge University Press, 2000), chap. 4.

ACKNOWLEDGEMENTS

We thank Takashi Kawashima and Pablo Blinder for valuable discussions and advice; Roy Hofi, Estar Regev and fish facility personnel. G.L. lab is supported by the Israel Science Foundation (#349/21); Hedda, Alberto, and David Milman Baron Center for Research on the Development of Neural Networks; Wolfe Family Center for Research on Neuroimmunology and Neuromodulation; Sagol Center for Research on the Aging Brain; and Maurice and Vivienne Wohl Biology Endowment and Foundation for Higher Education and Culture. P.R. was supported by a research grant for a student fellowship from the Benoziyo Endowment Fund for the Advancement of Science and by the Weizmann–CNRS Collaboration Program. G.L. is an incumbent of the Elias Sourasky Professorial Chair.

AUTHOR CONTRIBUTIONS

Conceptualization, P.R. and G.L.; Methodology, P.R. Investigation, P.R., O.R. and G.L.; Resources, P.R., Formal analysis, P.R. and O.R.; Writing-original draft, P.R. and G.L.; Writing-review and editing, P.R., G.L., and O.R.; Visualization, P.R.; Funding acquisition, G.L.; Project administration, P.R. and G.L.

MATERIALS AND METHODS

Husbandry and housing conditions of experimental animals

All experiments using zebrafish were approved by the Weizmann Institute's Institutional Animal Care and Use Committee (Application number 00590123-3 and 16970919-3). Zebrafish were maintained and bred using standard protocols and according to FELASA guidelines.

Transgenic animals

The following transgenes were used in this study: *Tg(l-fabp:DBP-eGFP)*,*Tg(kdrl:eGFP), Tg(oxt:gal4-VP16; UAS:NTR-mCherry; l-fabp:DBP-eGFP/kdrl:eGFP), Tg(oxt:gal4-VP16; UAS:CoChR-tdTomato; l-fabp:DBP-eGFP/kdrl:eGFP).* Larvae that were to be imaged were kept in the Danieau's buffer with 0.003% PTU from 24hpf till the day of the experiment.

Organism/ Recombinant DNA	**Allele number**	**ZFIN ID**
Tg(kdrl:eGFP)	s843	ZDB-ALT-050916-14
Tg(l-fabp:DBP-EGFP)	lri500	ZDB-ALT-120118-1
Tg(oxt:Gal4; cmlc2:EGFP)	wz06	ZDB-ALT-171113-2
Tg(UAS:NTR-mCherry)	jh17	ZDB-ALT-110222-4
Tg(UAS:CoChR-tdTomato)	u332	ZDB-TGCONSTRCT-190226-2

In-vivo imaging of live zebrafish

Six days post fertilization (dpf) zebrafish larvae were immobilized with a 30s incubation with 1mg/ml alpha-bungarotoxin followed by a quick wash in E3 media and mounted in 0.8% low-melt agarose in a custom molded 3cm plate filled with 2% agarose. The plate was filled with 3ml E3 media prior to imaging. Samples were excited using the Zeiss LSM7 Multi-Photon Microscope with a pulsed laser (Coherent Chameleon) tuned to 870nm set at a 4-6% laser intensity (max. 210mW) through a 20x water immersion Pln Apochromatic Lens. Emitted light was detected through the BiG detector after passage through a BP500-550 filter. Line scans were obtained by manually defining a single-pixel scan path (pixel scaling of 0.03um) as required which was then scanned for a pre-defined number of frames using the Galvanometric scanning head.

516 **Osmotic challenge, cell ablation and pharmacological treatments**

517 Zebrafish were osmotically challenged using 50% instant ocean salt (17.5 gr/l; Instant Ocean
518 Sea Salt, Aquarium Systems) dissolved in E3 media (5.03mM NaCl, 0.17mM KCl, 0.33mM
519 $CaCl_2.2H_2O$, 0.33mM $MgSO_4.7H_2O$). Oxytocin neurons were ablated by treating 5 dpf
520 *Tg(oxt:gal4-VP16; UAS:NTR-mCherry)* larvae on the background of either *Tg(l-fabp:eGFP)*
521 or *Tg(kdrl:eGFP)* with 5uM Nifurpirinol (NFP; LGC, 13411-16-0) for 18h at 28.5^0C in E3
522 media. Larvae where then washed for two hours in E3 media before live imaging. Controls for
523 the experiment were *Tg(oxt:gal4-VP16; UAS:NTR-mCherry)* negative siblings which were
524 also treated with NFP to account for the effects of the drug itself.

525 Oxytocin receptor signaling was attenuated by treating 6 dpf *Tg(l-fabp:eGFP)* or
526 *Tg(kdrl:eGFP)* larvae with 100mM Oxtr antagonist L-368,899 (No.2641, Tocris Bioscience)
527 dissolved in E3 media for 1hour at 28.5^0C followed by live imaging.

528 Tgfβ receptor inhibition was carried out by treating 4 dpf *Tg(l-fabp:eGFP)* or *Tg(kdrl:eGFP)*
529 larvae with 25uM SB431542 (S4317, Sigma-Aldrich) dissolved in DMSO for 48h at 28.5^0C
530 followed by live imaging.

531 To slow down blood flow in the brain/pituitary, 6 dpf *Tg(l-fabp:eGFP)* or *Tg(kdrl:eGFP)*
532 larvae were incubated in a-bungarotoxin for 150 seconds followed by a wash and live imaging.

533 **Optogenetic activation of oxytocin neurons**

534 Adult *Tg(oxt:gal4-VP16)* were crossed with *Tg(l-fabp:eGFP)* or *Tg(kdrl:eGFP)* and the
535 resultant embryos were injected with 40ng/ul of UAS:CoChR-tdTomato (Addgene; plasmid
536 #124233) construct and 40ng/ml of Transposase mRNA at the single-cell stage. Larvae were
537 visually sorted at 5dpf for strong expression of tdTomato in the oxytocin neurons under a
538 fluorescent stereo microscope. Control larvae were siblings that were not injected with the
539 UAS:CoChR-tdTomato construct. All experimental cohorts were grown in an incubator at
540 28.5^0C in the dark.

541 Hypophyseal capillary was imaged under basal conditions, with minimal light activation of the
542 neurons, followed by 10 minutes of rest. Oxytocin neurons were then stimulated for 5 seconds
543 with a 470nm Fiber-coupled LED (ThorLabs Inc,USA) through a fiber optic cannula (400um,

0.39NA; ThorLabs) placed near the head of the larvae at 1.5 mW/mm2, followed immediately by live imaging of the hypophyseal capillary only.

Monitoring and analysis of blood flow velocity

Arbitrary line scans with a length of approx. 20 um along the vessel length were obtained at 133 Hz in the *Tg(l-fabp:DBP-eGFP)* transgenic line. These line scans were then combined into a multi-frame time-displacement image (kymograph). Two signals were derived from two different points on the displacement axis, and along the time axis. These signals were a representation of the fluctuation in fluorescence intensities across time. Independently, each of these signals gives a measure of the number of red blood cells (RBCs) flowing through the cross-sectional area of the hypophyseal capillary per unit time. On comparing the two signals from each RBC, taken at points x1 and x2, we get the displacement of the RBC within the time frame between t1 and t2. Using these coordinates, the slope of each RBC was computed, and converted to velocity (**Fig. S1C**). The individual RBC velocities in the given kymograph were then plotted as a function of normalized displacement. With an optimal sampling rate of RBCs per second, individual velocities of the RBCs across time were used to obtain a power density spectrum to identify the frequencies at which the flow velocities oscillate. Changes between basal and treated conditions were also depicted as a change in power of particular frequencies or a shift in the frequency itself using a fast Fourier transform (FFT).

Capillary diameter measurements

To measure capillary diameter, line scans were taken perpendicular to vessel length at 133 Hz in the *Tg(kdrl:eGFP)* line. The length of the line was approx. 40um, which covered both ends of arms of the hypophyseal capillary. These line scans were then combined into a multi-frame time-displacement image (kymograph), where each line perpendicular to the x-axis represents a single diameter trace at the corresponding time (**Fig. S1D**). Signals derived from each line corresponding to time values on the x-axis were plotted to obtain two Gaussians each representing the left or right vessel wall. Inner and outer diameter measurements were obtained by measuring the distance between the inner and outer Full-Width Half-Maxima (FWHM) values of these Gaussians. This diameter measured is then converted from pixels to microns and plotted as the final graph as the diameter changes across time for both basal and treated conditions.

575 **Vascular permeability assay**

576 Permeability was visualized and quantified using the *Tg(l-fabp:DBP-EGFP)* reporter by
577 employing fluorescence recovery after photobleaching (FRAP) to determine the average
578 recovery half-time ($T_{1/2}$) of the extravasated DBP-EGFP signal. This was carried out by
579 defining two circular regions of interest (ROIs), each of 5µm in diameter, on either side of the
580 hypophyseal capillary. A line scan path (pixel size 0.06um) was drawn perpendicular to
581 direction of flow, through the vessel, and through the centers of the two ROIs. Basal
582 measurements of raw fluorescence were obtained, followed by bleaching the ROI in the area
583 within the hypophyseal loop (**Fig. 6A**). Photobleaching was performed at 100% laser power
584 (approx. 3500mW) for 2.2s at 870nm, followed by the acquisition of the recovery of
585 fluorescence along the line scan path. Raw fluorescence was extracted directly by Zen and was
586 exported to MATLAB to calculate $T_{1/2}$ values. $T_{1/2}$ was calculated by fitting an exponential
587 curve to the recovery florescence and calculating the intercept on the time axis at the point of
588 50% of the maximal fluorescence. The unbleached ROI was used as a control for unintentional
589 bleaching, and basal fluorescence was used to validate the maximal fluorescence values after
590 recovery.

591 **Whole-mount immuno-fluorescence, HCR mRNA in-situ hybridization**

592 Six day-old larvae were fixed in 4% PFA, followed by PBST washes and overnight incubation
593 with 100% Methanol at -20C. Larvae were washed with PBST (0.5% Tween-20 in 1x
594 Phosphate Buffered Saline), incubated in blocking solution for 1 hour at room temperature,
595 followed by overnight incubation at 4C with Guinea Pig anti-oxytocin antibody (Peninsula
596 Laboratories International Inc., CA, USA, no. T-5021) in a blocking solution (5% goat serum
597 in PBST). Larvae were washed with PBST, and then incubated for 4 hours at room temperature
598 with Mouse anti-guinea pig Cy5 secondary antibody (Jackson ImmunoReasearch Laboratories,
599 PA, USA) followed by PBST washes.

600 Hybridization chain reaction (HCR) in-situ v3.0 probes for *c-fos mRNA* were custom designed
601 and synthesized by Molecular Instruments (USA). In-situ hybridization was performed
602 according to Chen et al. (*15*) .

603 Larvae were then mounted in 75% glycerol and imaged with a 40x oil immersion lens using
604 the Zeiss LSM800 confocal setup using the appropriate emission/excitation filters.

605 **FACS Sorting and qRT-PCR**

606 Five adult pituitaries of the *Tg(kdrl:eGFP)* transgenic line were dissected into Ca^{2+} free
607 Ringer's solution (116 mM NaCl, 2.9 mM KCl, 5.0 mM HEPES, pH 7.2), followed by a 30
608 minute incubation in 1X TrypLE Express (Gibco, 12604-013). Pituitaries were then mashed
609 onto a 40um cell stainer and flushed into an Eppendorf using 500ul suspension buffer (L15
610 media without phenol red (Gibco, 21083-027), 1% FBS, 0.5% pen-strep solution). 25ul of
611 20ug/ml DAPI was added, and the cells were sorted into three populations: all pituitary cells
612 (GFP+ and GFP-), endothelial cells only (GFP+), and endothelial depleted (GFP-).
613 populations. Cells were collected in a lysis buffer (0.3% NP-40, 0.1% FBS, 1% RNase
614 Inhibitor) and converted into cDNA directly (Takara, #RR036A). qRT-PCR was performed
615 with 200cells per well and three technical triplicates using the following gene-specific primers:

Gene	Forward Primer (5' -> 3')	Reverse Primer (5' -> 3')
B-actin	TCTTCACTCCCCTTGTTCACAA	TGCCAACCATCACTCCCTGA
kdrl	TCCCCTTACCCTGGCTTACA	GTGGGCCTCTGAGATGGTTC
pdgfrB	TTGTCGAGGCAACAGCGTAT	CTGCGAGCCGTTGATTTGAG
oxtra	TTCTCCGTGCAGATGTGGTC	TAGAGCGTGGAGCAGCAAAA
oxtrb	TACATCATCTGCTGGACGCC	TGCATGAGATCCCGGAACAG

616

617 **Codes**

618 All algorithms to measure velocity, diameter and permeability were custom written on
619 MATLAB (Mathworks, USA) and are available on request.

620 **Statistical analysis**

621 All statistical analyses and graphing were performed using PRISM 10.2 (GraphPad Software
622 Inc, San Diego, USA). Data tables were exported from MATLAB to Prism were required. The
623 normality of the data sets were tested using the Shapiro-Wilk test, and parametric/non-
624 parametric tests were carried out with either a Paired t-test, Mann-Whitney test or the Wilcoxon
625 test for paired samples. All the tests were two-tailed analyses. Welch's ANOVA with Geisser-
626 Greenhouse corrections or Kruskal-Wallis tests was carried out where appropriate with
627 multiple comparisons (Dunnett's, Dunn's or Tukey's). Significance thresholds for all analyses
628 were set at a 0.05 threshold and p-values were corrected for multiple comparisons were
629 necessary. No data points were excluded as outliers in all analyses.

Theoretical resolution of hypophyseal vascular response

Expressing Poiseuille's law for fluid flow through a vessel in terms of flow velocity and vessel radius, we get:

$$\text{(a) } V = \frac{r^2 \Delta p}{8\mu L}$$

where r is the radius of the vessel, V is the velocity, Δp is the pressure difference between the two ends of the vessel, μ is the viscosity, and L is the length of the vessel (*54*).

An increase in velocity should be accompanied by an increase in radius of the vessel. However, in response to the stimulation of oxytocin neurons by osmotic challenge, we see an increase in velocity accompanied by a decrease in radius. To resolve this paradox, we looked closer into the geometry of the vascular microcircuit and reduced it to a function of their vascular resistances (**Fig. 2G**).

$$R_{tot} = R_1 + \frac{R_2^2}{2R_2}$$

$$\text{Total Flow, } Q_{tot} = \frac{\Delta p}{R_{tot}} = \frac{\Delta p}{R_1 + \frac{R_2}{2}}$$

Where R_{tot}, R_1, and R_2 are the total resistance, arterial and capillary resistance respectively, and Q_{tot} is the total flow rate.

Pressure difference in the capillary, $\Delta p_2 = Q_{tot} R_{par}$

$$\Delta p_2 = \frac{\Delta p}{R_1 + \frac{R_2}{2}} \cdot \frac{R_2}{2}$$

$$V_2 = \frac{Q_2}{A_2} = \frac{\Delta p}{2R_1 + R_2} \cdot \frac{1}{\pi r^2}$$

Breaking down the denominator and expressing resistance in terms of radius, we get:

$$2R_1 r_2^2 + R_2 r_2^2 = \frac{8\mu}{\pi}\left(\frac{2L_1 r_2^2}{r_1^4} + \frac{L_2}{r_2^2}\right)$$

Where a is the radius of the artery, L_1 and L_2 are the lengths of the artery and capillary, respectively.

Substituting the above equation back in the original equation, and $L_1 / L_2 = 2.5L_2$:

$$\text{(b) } V_2 = \frac{r_1^4 r_2^2 \Delta p}{8\mu L_2 (5r_2^4 + r_1^4)}$$

From this equation, given our experimental data, we derived a range of Δp values by pair matching different combinations of mean velocity and radii from out experimental cohorts. A velocity vs radius graph was then plotted using a range of radii with the above pre-defined sets of values for each curve (**Fig. 2H**).

659 **LEGENDS TO FIGURES**

660 **Figure 1. Physiological osmotic challenge increases local hypophyseal blood flow**
661 (**A**) Representative image and scheme showing the hypophyseal neurovascular interface of the
662 transgenic 6-day-old zebrafish larval *Tg(oxt:eGFP;kdrl:mCherry)*. Oxytocin axonal termini
663 and blood vessels are labelled in green and red respectively. (**A, right**) Schema depicting the
664 stereotypic anatomical structure of the hypophyseal artery (HyA), capillary (HyC) and vein
665 (HyV), as well as the anterior mesenchephalic central artery (AMCtA), which was used as a
666 control. Arrows indicate the positions of line scans imaging through and across the vessel were
667 employed to acquire changes in capillary diameter and red blood cell (RBC) velocity traces.
668 (**B-C**) Transgenic *Tg(oxt:eGFP)* zebrafish larvae with labeled oxytocin (OXT) neurons were
669 incubated with hyperosmotic solution equivalent to 50% seawater (17.5 ppt) followed by in-
670 situ hybridization of the activity-dependent *c-fos mRNA.* Representative image of a single z-
671 plane (**B**) showing increased *c-fos* expression in OXT neurons following the osmotic challenge
672 quantified (**C**) as the number of *c-fos* positive OXT neurons expressing cells ($p < 0.0001$, Mann-
673 Whitney test, naïve n=9, OC=10). Scale bar, 20um.
674 (**D-G**) Representative blood flow traces in the HyC (**D**) at basal conditions and following the
675 osmotic challenge (OC) which led to increased mean RBC velocities in the HyC (**E,** p=0.001,
676 Paired t-test, n=9) and higher variability of velocities measured by spread of individual
677 velocities around the mean (**F,** p=0.0039, Wilcoxon test, n=9). Single-sided amplitude spectra
678 of the velocities (**G**) indicate an increase in amplitudes for frequencies less than 2Hz following
679 the OC.
680 (**H-K**) Osmotic challenge induced no changes to the blood flow traces (**H**), mean velocity (**I**,
681 p=0.2296, Paired t-test, n=7), variability in velocities (**J**, p=0.2669, Paired t-test, n=7), or any
682 changes in the spectra (**K**) in the AMCtA which served as control for the specific effect of the
683 OC.
684

685 **Figure 2. Hypophyseal vascular response is determined by it's geometry.**
686 Changes in capillary diameter in the HyC (**A-C**) and AMCtA (**D-F**).
687 (**A-F**) Representative diameter traces of HyC (**A**) and AMCtA (**D**). Mean diameter of the
688 capillary significantly decreases after OC (**B**, p=0.0156, Wilcoxon test, n=7), as further shown
689 as a ratio of diameter change to basal diameter (**C**, p=0.0006, Mann-Whitney test, n=7).
690 (**D-F**) OC did not affect the mean diameter (**E**, p=0.3076, Paired t-test, n=7), or the ratio of
691 diameter change to basal diameter (**F**, p=0.6900, Mann-Whitney test, n=7) of the AMCtA.

692 (**G**) The predicted relationships between hypophyseal diameter and velocity was theoretically
693 resolved according to Poiseuille's law for viscous fluids by representing the individual
694 components the hypophyseal vascular microcircuit having an inlet-outlet pressure differences
695 (Δp). The corresponding resistance (R), length (L), and radius (r) of the hypophyseal artery
696 (HyA) and capillary (HyC) are indicated. The resulted equation of hypophyseal flow velocity
697 (V_2) as a function of the above parameters is shown (**Fig. 2G,** for details, see '*Methods*'
698 section).
699 (**H**) A range of pressure differences, Δp, was determined by multiple random matches between
700 velocity and radii values that were obtained experimentally. This range was plugged into the
701 resolved V_2 equation resulting three curves indicating the relationship between velocity and
702 radii of the hypophyseal capillary for a given Δp. The measured average velocities before and
703 after osmotic challenge (OC) are indicated by dashed lines (**H**). The point of intersection
704 between the corresponding basal and OC velocities and the curves for a given Δp are indicated
705 by the green and red Xs (**H'**). A corresponding increase in velocity following an OC requires a
706 small increase in pressure and vasoconstriction (solid line) or a large decrease in radius (**H'**,
707 dashed line).
708
709 **Figure 3. Ablation of oxytocin neurons attenuates vascular response to an osmotic**
710 **challenge.**
711 (**A**) Schema representing the transgenic *Tg(oxt:gal4;UAS:NTR-mCherry)* larvae, in which
712 oxytocin neurons express the nitroreductase (NTR) enzyme which reduces the drug nifurpirinol
713 (NFP) into a cytotoxic compound causing specific oxytocinergic cell death.
714 (**B-C**) *Tg(oxt:gal4;UAS:NTR-mCherry)* larvae were treated for 18 hours with 5uM NFP and
715 immune-stained with and antibody directed to endogenous OXT protein. NTR- (control) and
716 NTR+ (Ablated) siblings were treated with NFP, followed by anti-OXT antibody staining.
717 Representative confocal z-stacks images show a reduction of OXT protein in
718 neurohypophyseal axonal projections following NFP treatment of NTR-positive larvae (**B**).
719 Scale bar, 10um. Quantification of OXT-immunoreactive fluorescence shows significantly
720 reduction of OXT in neurohypophyseal termini in the NTR+ cohort (**C**, $p<0.0001$, Mann-
721 Whitney test, control n=19, treated n=19).
722 Blood flow velocity traces representing the osmotic challenge (OC) increase in hypophyseal
723 blood flow velocity in control (**D**), but not OXT-ablated (**E**) larvae. (**F**) Mean velocity after OC
724 was increased in NTR- larvae ($p=0.0046$, Paired t-test, n=7), but not in their NTR+ siblings

725 (p=0.0947, Paired t-test, n=7). (**G, H**) Single sided amplitude spectra of the NTR+ cohort show
726 no difference before and after OC as compared to the controls. Variability in velocity was
727 increased after OC in NTR- cohort also (**I**, p=0.0081, Paired t-test, n=7), but not in their NTR+
728 siblings (**I**, p=0.5781, Wilcoxon test, n=7).
729 (**J-K**) Representative diameter traces before and after osmotic challenge showing capillary
730 vasoconstriction of control NTR- larvae (**J**) compared to vasodilation of ablated NTR+ siblings
731 (**K**).
732 **(L)** Following OC, the hypophyseal capillary of NTR- larvae showed a decrease in diameter
733 (p= 0.0156, Wilcoxon test, n=7) while NTR+ larvae showed an increase in diameter (p=0.0045,
734 Paired t-test, n=7). The ratio between diameter change to basal diameter after OC (**M**) was
735 significantly different between the NTR- and NTR+ cohorts (p<0.0001, Dunn's multiple
736 comparison, NTR- n=7, NTR+ n=7).
737 (**N-P**) Mean velocity (p=0.3941, Paired t-test, n=7), variability of velocity (p=0.6983, Paired
738 t-test, n=7) and diameter (p=0.5249, Paired t-test, n=7) of the AMCtA did not change after OC
739 in NTR+ larvae treated with NFP. The control NTR- larvae treated with NFP also did not show
740 any difference in mean velocity (p=0.3095, Paired t-test, n=7), variability of velocity
741 (p=0.5781, Wilcoxon test, n=7) and diameter (p=0.4430, Paired t-test, n=7) in the AMCtA after
742 OC.
743
744 **Figure 4. Hypophyseal blood flow is regulated by oxytocin signaling**
745 (**A, B**) Representative hypophyseal blood flow velocity traces before and after osmotic
746 challenge (OC). Larvae treated with the Oxtr antagonist (Oxtr ant.) L-368,899 show no change
747 in response to OC as compared to their control sibling. Mean velocity (**C**) after OC in the oxtr
748 ant- cohort show an increase (p=0.0033, Paired t-test, n=7), that is not observed in L-368,899
749 antagonist treated siblings (p=0.2509, Paired t-test, n=7). (**D, E**) Single sided amplitude spectra
750 show that while the frequency spectra of a control cohort were affected the OC, larvae treated
751 with the Oxtr antagonist show no difference. Variability in velocities (**F**) was increased
752 following OC (p=0.0213, Paired t-test, n=7), but not in Oxtr antagonist- treated siblings
753 (p=0.7195, Paired t-test test, n=7).
754 (**G, H**) Representative diameter traces showing vasoconstriction following osmotic challenge
755 of control sibling but not in larvae treated with Oxtr antagonist (**I**) No significant change in
756 the mean capillary diameter of the Oxtr antagonist-treated larvae which were subjected to OC
757 (p=0.3892, Paired t-test, n=7) compared to a decrease in diameter in the control cohort
758 (p=0.0001, Paired t-test, n=7). (**J**) The ratio between diameter change to basal diameter after

759 OC showed a significant difference between the control and antagonist-treated cohorts
760 (p=0.0010, Dunn's multiple comparison, Oxtr ant- n=7, Oxtr ant+ n=7).
761 (**K-M**) Mean velocity (p=0.2008, Paired t-test, n=7), variability of velocity (p=0.8040, Paired
762 t-test, n=7) and diameter (p=0.8509, Paired t-test, n=7) of the AMCtA did not change after OC
763 in Oxtr ant+ larvae. The control Oxtr ant- larvae also did not show any difference in mean
764 velocity (p=0.8573, Paired t-test, n=7), variability of velocity (p=0.8533, Paired t-test, n=7)
765 and diameter (p=0.9422, Paired t-test, n=7) in the AMCtA after OC.
766
767 **Figure 5. Optogenetic stimulation of oxytocin neurons increases hypophyseal blood flow**
768 **and is dependent on oxytocin signaling**
769 (**A-B**) Scheme representing the Gal4-UAS system foe expression of a blue light- activated
770 channel rhodopsin (*UAS:CoChR-tdTomato*) in oxytocin (OXT) neurons using *Tg*(oxt:Gal)
771 transgenic driver. (**B**) Representative single z-plane confocal image of oxytocin neurons
772 expressing CoChR-tdTomato. Scale bar, 20um.
773 (**C, D**) Representative blood flow velocity traces before and after light stimulation in larvae
774 expressing CoChR show an increase in blood flow velocity as compared to their control sibling.
775 (**E**) Blue light stimulation of CoChR+ larvae led to an increase in mean peak blood flow
776 velocity (p=<0.0001, Paired t-test, n=7). Control CoChR- siblings were not responsive to the
777 light stimulation (p=0.4688, Wilcoxon test, n=7).
778 (**F**) The ratio between velocity change to basal velocity after light stimulation of the CoChR+
779 cohort increased as compared to their CoChR- sibling cohort (p=0.0225, Dunn's multiple
780 comparison, CoChR- n=7, CoChR+ n=7).
781 (**G**) Representative blood flow velocity traces before and after light stimulation in larvae
782 expressing CoChR and treated with the Oxtr antagonist L-368,899 (Oxtr ant.).
783 (**H**) Mean velocity after light stimulation in the CoChR+ Oxtr ant+ larvae show an increase
784 (p=0.0313, Wilcoxon test, n=7), which was also observed in their CoChR+ Oxtr ant- siblings
785 (p=<0.0001, Paired t-test, n=7). (**I**) The ratio between velocity change to basal velocity after
786 light stimulation in the vehicle-treated CoChR+ was significantly larger as compared to their
787 CoChR+ siblings treated with L-368,899 (p=0.0287, Dunn's multiple comparison, Oxtr ant-
788 n=7, Oxtr ant+ n=7).
789 (**J-K**) Representative diameter traces before and after light stimulation in larvae expressing
790 CoChR show an increase in blood flow velocity as compared to their control sibling.
791 (**L-M**) Mean diameter after light stimulation in the CoChR+ larvae show a decrease (p=0.0043,
792 Paired t-test, n=7), that is not observed in their CoChR- siblings (p=0.3349, Paired t-test, n=7).

793 The ratio between diameter change to basal diameter after light stimulation in the CoChR+
794 cohort is lower as compared to their CoChR- sibling cohort (p=0.0047, Dunn's multiple
795 comparison, CoChR- n=7, CoChR+ n=7).
796 (**N**) Representative diameter trace before and after light stimulation in larvae expressing
797 CoChR and treated with the Oxtr antagonist L-368,899.
798 (**O**) Light stimulation of CoChR+ larvae led to a decrease in mean capillary diameter
799 (p=0.0010, Paired t-test, n=7). The capillary diameter of the antagonist-treated CoChR+ larvae
800 did not respond to the optogenetic activation (p=0.6043, Paired t-test, n=7).
801 (**P**) The ratio between diameter change to basal diameter after light stimulation of the
802 antagonist-treated CoChR+ larvae were significantly lower as compared to vehicle-treated
803 CoChR+ sibling cohort (p=0.0060, Dunn's multiple comparison, Oxtr ant- n=7, Oxtr ant+
804 n=7).
805 Dashed lines in all representative traces indicate a LOWESS curve fitted to the data with a
806 smoothing window of ten points.
807
808 **Figure 6. Hypophyseal vascular permeability is regulated by oxytocin signaling**
809 (**A**) Graphical representation of the permeable hypophyseal capillary visualized in the *Tg(l-*
810 *fabp:DBP-eGFP)* larvae. (**A'**) Scheme depicting the hypophyseal capillary permeability assay
811 in which fluorescent recovery after photobleaching (FRAP) of the extravasated DBP-EGFP
812 signal the *Tg(l-fabp:DBP-EGFP)* reporter was measured in a region of interest (ROI) within
813 the hypophyseal capillary loop (red circle) compared to a control ROI outside of the loop. (**B**)
814 A kymograph representing a line scan across time showing the bleached and unbleached ROIs
815 on either side of the hypophyseal capillary, which is marked by dashed lines. The bleaching
816 time point is marked by an arrowhead. (**C**) Average FRAP recovery half-time $T_{1/2}$ was
817 decreased after osmotic challenge (OC) (p<0.0001, Paired t-test, n=8).
818 (**D**) Kymographs representing FRAP traces of naïve (unchallenged) larva displaying vehicle-
819 treated control larva and larva treated with 25 μM of the Tgfβ receptor inhibitor SB431542
820 (TgfβR in.). The bleaching time point is marked by an arrowhead. Higher intensity images of
821 the FRAP kymographs before and after photobleaching are shown on the right (**D'**).
822 (**E**) The basal $T_{1/2}$ values of SB431542-treated larvae were significantly higher than their
823 vehicle-treated siblings (p<0.0001, Dunnett's multiple comparison, TgfβR inh.- n=7, TgfβR
824 inh.+ n=7). Larvae treated with SB431542 exhibit a decrease in $T_{1/2}$ values after OC (p=0.0002,
825 Paired t-test, n=7) as do their vehicle-treated control larvae (p=0.0012, Paired t-test, n=7).

826 (**F**) Mean blood flow velocity values following OC was increased in larvae that were treated
827 with the TgfβR inhibitor ($p<0.0001$, Paired t-test, n=7) as do their vehicle-treated controls
828 ($p=0.0007$, Paired t-test, n=7).
829 (**G**) Representative kymographs of larvae exhibiting basal versus reduced blood flow.
830 (**H**) Application of 1 mg/ml of α-bungarotoxin for 30 seconds immobilizes larvae without
831 affecting blood flow velocity (basal), whereas incubation with α-bungarotoxin for 150 seconds
832 reduced mean blood flow velocity values ($p<0.0001$, Paired t-test, n=13).
833 (**I**) Reduction in blood flow velocity did not affect capillary permeability as indicated by FRAP
834 measurements of $T_{1/2}$ values ($p=0.0854$, Paired t-test, n=13).
835 (**J**) Hypophyseal capillary permeability was monitored at 20 mins intervals before and after the
836 application of Oxtr antagonist. A significant increase in $T_{1/2}$ after 40 and 60 mins of antagonist
837 treatment ($p=0.8090$, Basal *vs*. 20min; $p=0.0004$, Basal vs 40min; $p<0.0001$; Basal *vs*. 60min,
838 Dunnett's multiple comparison, n=7).
839 (**K**) The increment in capillary permeability which is induced by OC ($p<0.0001$, Paired t-test,
840 n=7) is blocked in larvae which were treated with the Oxtr antagonist L-368,899, showing no
841 change in $T_{1/2}$ after OC ($p=0.6147$, Paired t-test, n=7). In accord with Fig. 6J above, basal $T_{1/2}$
842 values of L-368,899- treated larvae were significantly higher than their untreated siblings
843 ($p<0.0001$, Dunnett's multiple comparison, Oxtr ant- n=7, Oxtr ant+ n=7).
844 (**L**) Optogenetic activation of OXT neurons was performed using oxt:Gal;*UAS:CoChR-*
845 *tdTomato* transgenic larvae, as described in the legend to Figure 5 following by FRAP-based
846 permeability measurements. Blue light stimulation of CoChR+ larvae led to a decrease in $T_{1/2}$
847 values ($p=0.0003$, Paired t-test, n=7). $T_{1/2}$ values were unaffected by light in CoChR- larvae
848 ($p=0.2559$, Paired t-test, n=7).
849
850 **Supplemental Fig. S1.**
851 (**A**) Scheme showing the production of DBP-eGFP under the liver promoter, L-fabp, in the
852 *Tg(l-fabp:DBP-eGFP)* transgenic line labelling the serum. Graphical depiction of experimental
853 workflow where either osmotic challenge or optogenetic stimulation is administered to the
854 zebrafish larvae followed by live *in-vivo* awake imaging (**A'**).
855 (**B**) Snap shot of the hypophyseal capillary loop of the *Tg(l-fabp:DBP-eGFP)* transgenic larvae
856 at 6dpf. Dark shadows are created by the red blood cells (RBCs) on a background of DBP-
857 eGFP labelled serum. (**C**)Kymograph shows red blood cells (RBCs) as black streaks on a
858 background of serum labelled with DBP-eGFP. Signals from each RBC, taken at points x1 and

x2, denote the displacement of the RBC within the time frame between t1 and t2. The velocity is given by the tangential derived from these components. (**D**) A kymograph across the blood vessel where each line perpendicular to the x-axis represents a single diameter trace at the corresponding time. $d_1(t)$ and $d_2(t)$ represent the position of the inner walls of the vessel on the displacement axis for a given time, t.

(**E**) Diameter of the hypophyseal artery shows no change after OC (p=0.1783, Paired t-test, n=7).

Supplemental Fig. S2.

(**A**) Adult pituitary sorted for all cells, endothelia only, and endothelia depleted populations show an enrichment of *oxtrb* mRNA in the endothelial population. *oxtra* mRNA was enriched in the endothelial depleted population but was still observed in low levels in the endothelia population. All comparisons of fold change are made with respect to the mRNA levels of the genes in the entire pituitary.

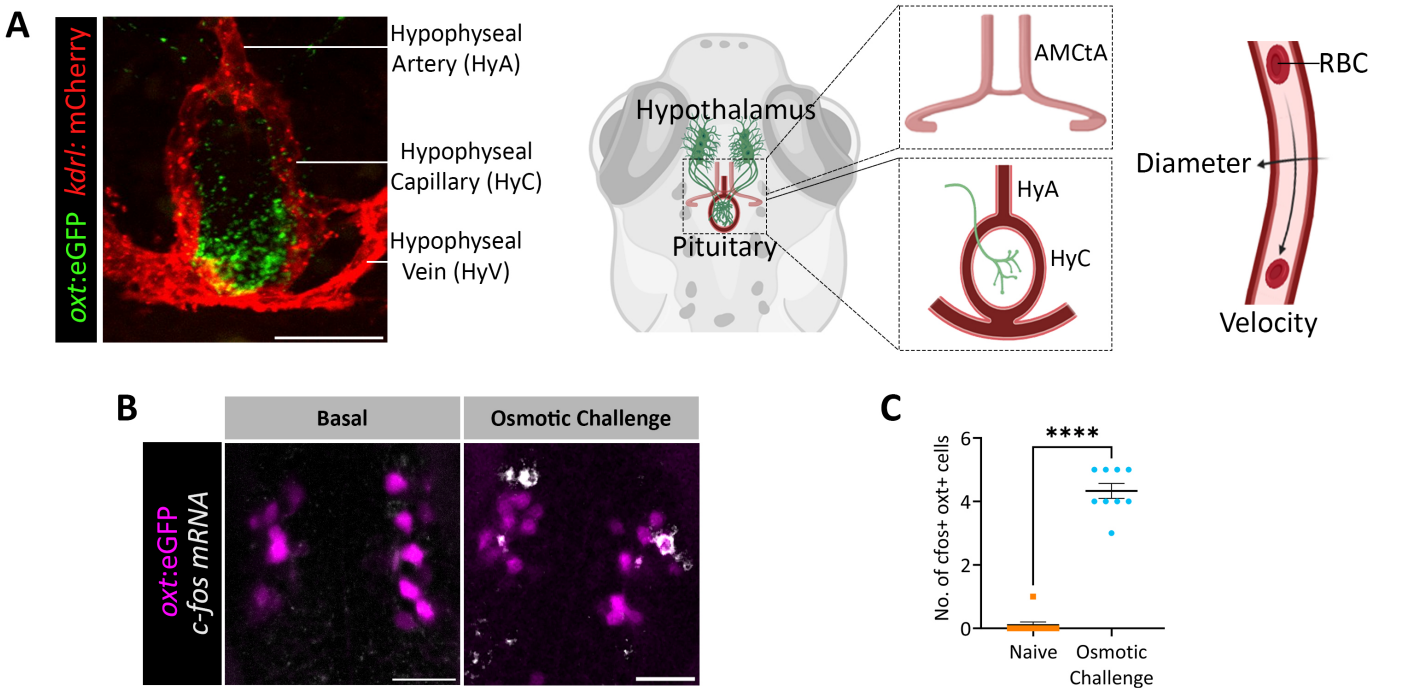

Hypophyseal Capillary (HyC)

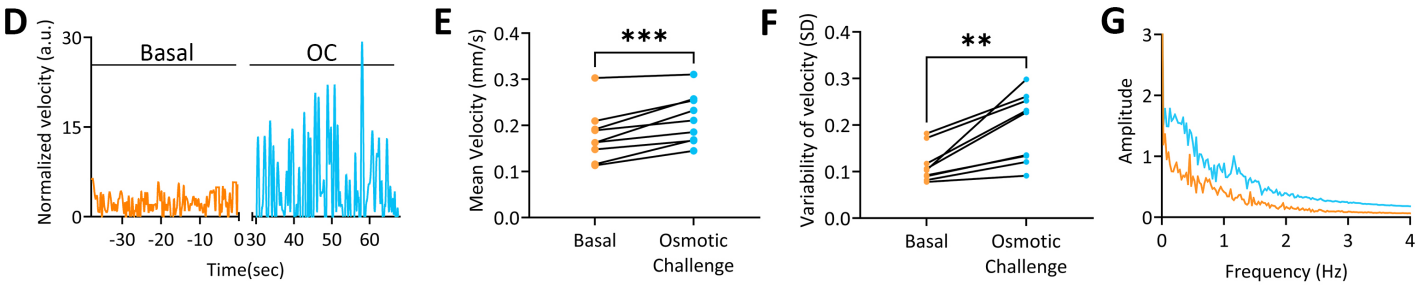

Anterior Mesencephalic Central Artery (AMCtA)

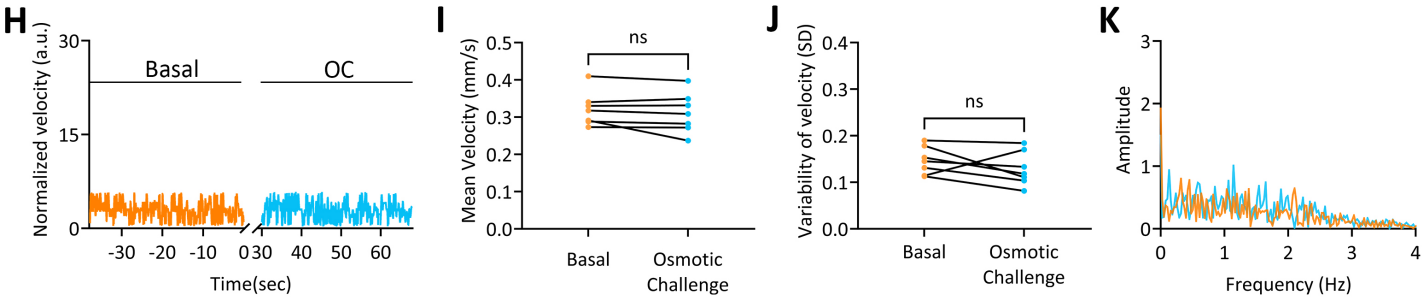

Figure 1

Hypophyseal Capillary (HyC)

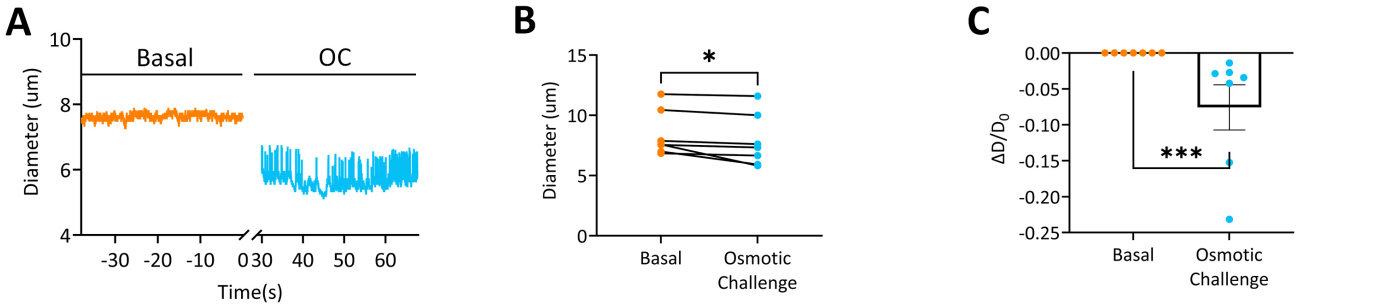

Anterior Mecencephalic Central Artery (AMCtA)

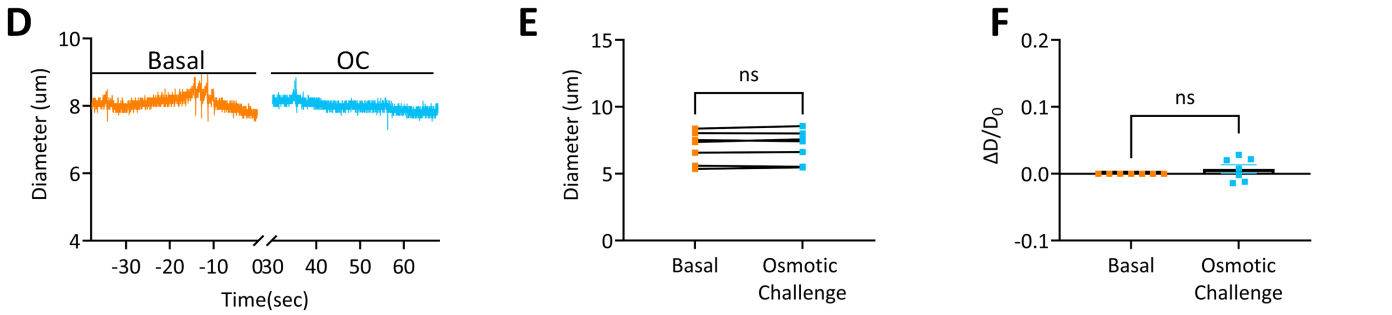

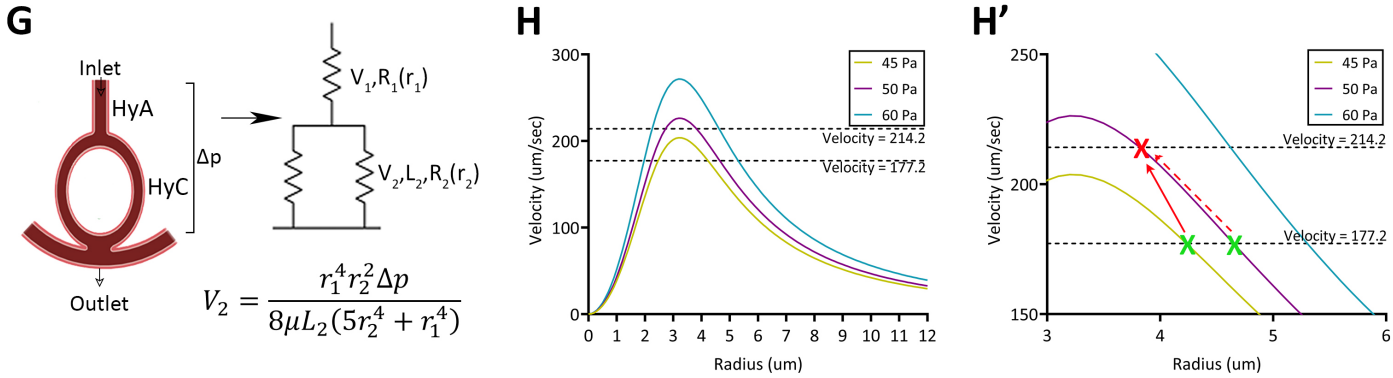

$$V_2 = \frac{r_1^4 r_2^2 \Delta p}{8\mu L_2 (5r_2^4 + r_1^4)}$$

Figure 2

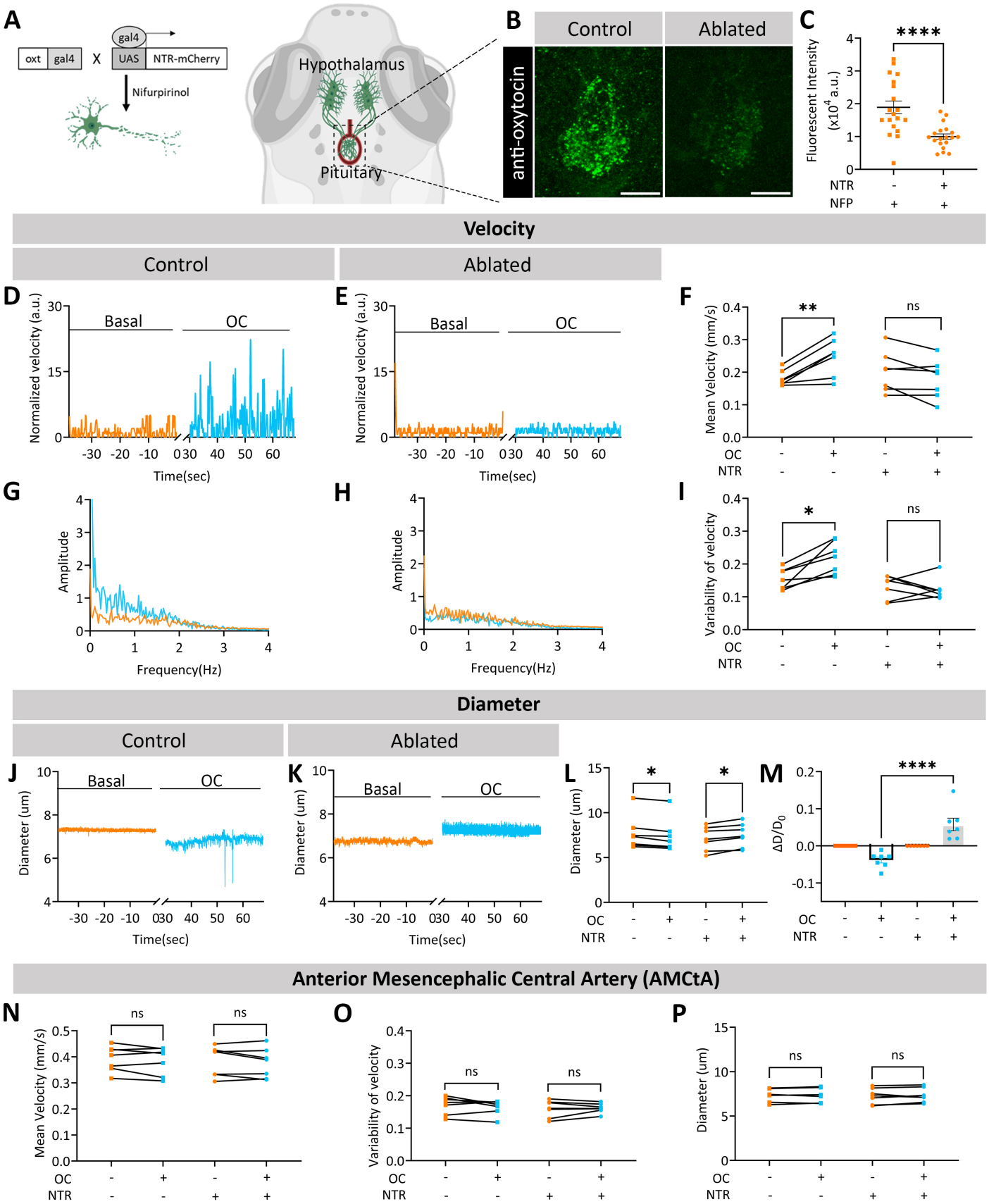
A
oxt
gal4
X
gal4
UAS
NTR-mCherry
Nifurpirinol
Hypothalamus
Pituitary
B
Control
Ablated
anti-oxytocin
C
Fluorescent Intensity (x10^4 a.u.)
****
NTR
NFP
Velocity
Control
Ablated
D
E
Normalized velocity (a.u.)
Basal
OC
Time(sec)
F
Mean Velocity (mm/s)
**
ns
OC
NTR
G
H
Amplitude
Frequency(Hz)
I
Variability of velocity
*
ns
Diameter
J
K
Diameter (um)
L
M
ΔD/D0
****
Anterior Mesencephalic Central Artery (AMCtA)
N
O
P
ns

Figure 3

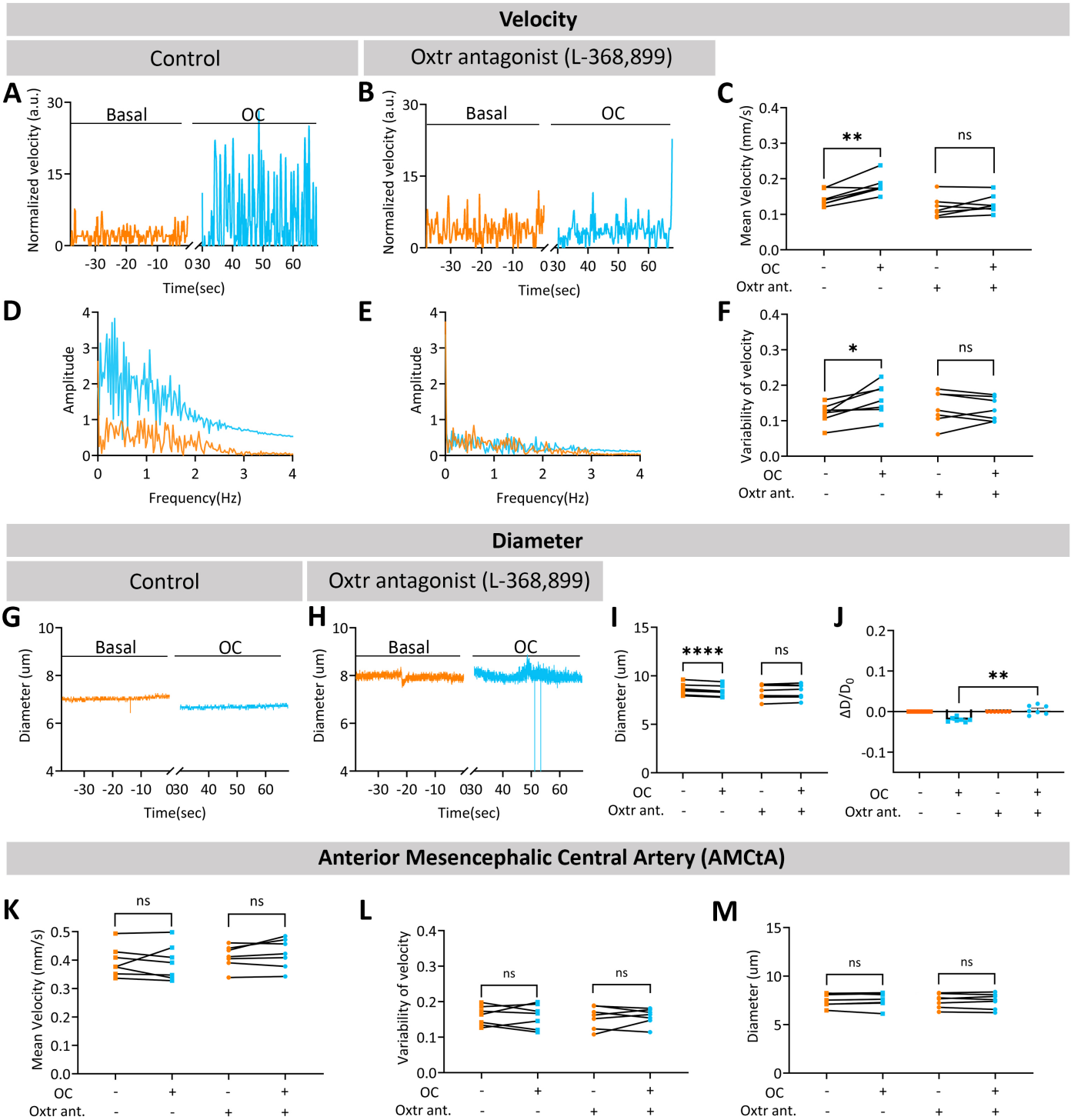
Velocity
Control
Oxtr antagonist (L-368,899)
A
Normalized velocity (a.u.)
Basal
OC
Time(sec)
B
C
Mean Velocity (mm/s)
**
ns
OC
Oxtr ant.
D
Amplitude
Frequency(Hz)
E
F
Variability of velocity
*
Diameter
G
Diameter (um)
H
I
****
J
ΔD/D0
Anterior Mesencephalic Central Artery (AMCtA)
K
L
M

Figure 4

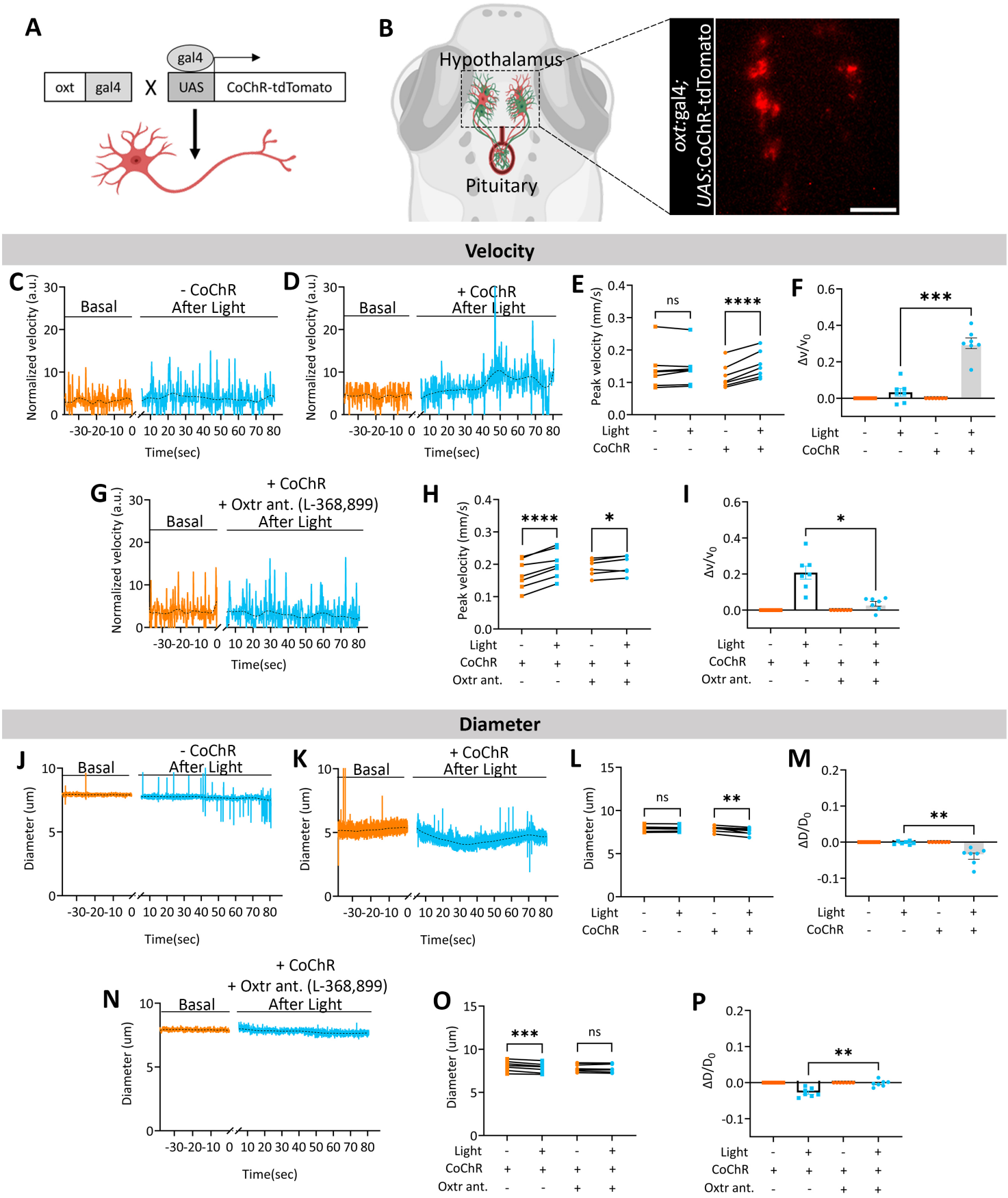
A
gal4
oxt
gal4
X
UAS
CoChR-tdTomato
B
Hypothalamus
Pituitary
oxt:gal4;
UAS:CoChR-tdTomato
Velocity
C
Basal
- CoChR
After Light
Normalized velocity (a.u.)
Time(sec)
D
Basal
+ CoChR
After Light
Normalized velocity (a.u.)
Time(sec)
E
Peak velocity (mm/s)
ns
****
Light
CoChR
F
Δv/v0
***
Light
CoChR
G
Basal
+ CoChR
+ Oxtr ant. (L-368,899)
After Light
Normalized velocity (a.u.)
Time(sec)
H
Peak velocity (mm/s)
****
*
Light
CoChR
Oxtr ant.
I
Δv/v0
*
Light
CoChR
Oxtr ant.
Diameter
J
Basal
- CoChR
After Light
Diameter (um)
Time(sec)
K
Basal
+ CoChR
After Light
Diameter (um)
Time(sec)
L
Diameter (um)
ns
**
Light
CoChR
M
ΔD/D0
**
Light
CoChR
N
Basal
+ CoChR
+ Oxtr ant. (L-368,899)
After Light
Diameter (um)
Time(sec)
O
Diameter (um)
***
ns
Light
CoChR
Oxtr ant.
P
ΔD/D0
**
Light
CoChR
Oxtr ant.

Figure 5

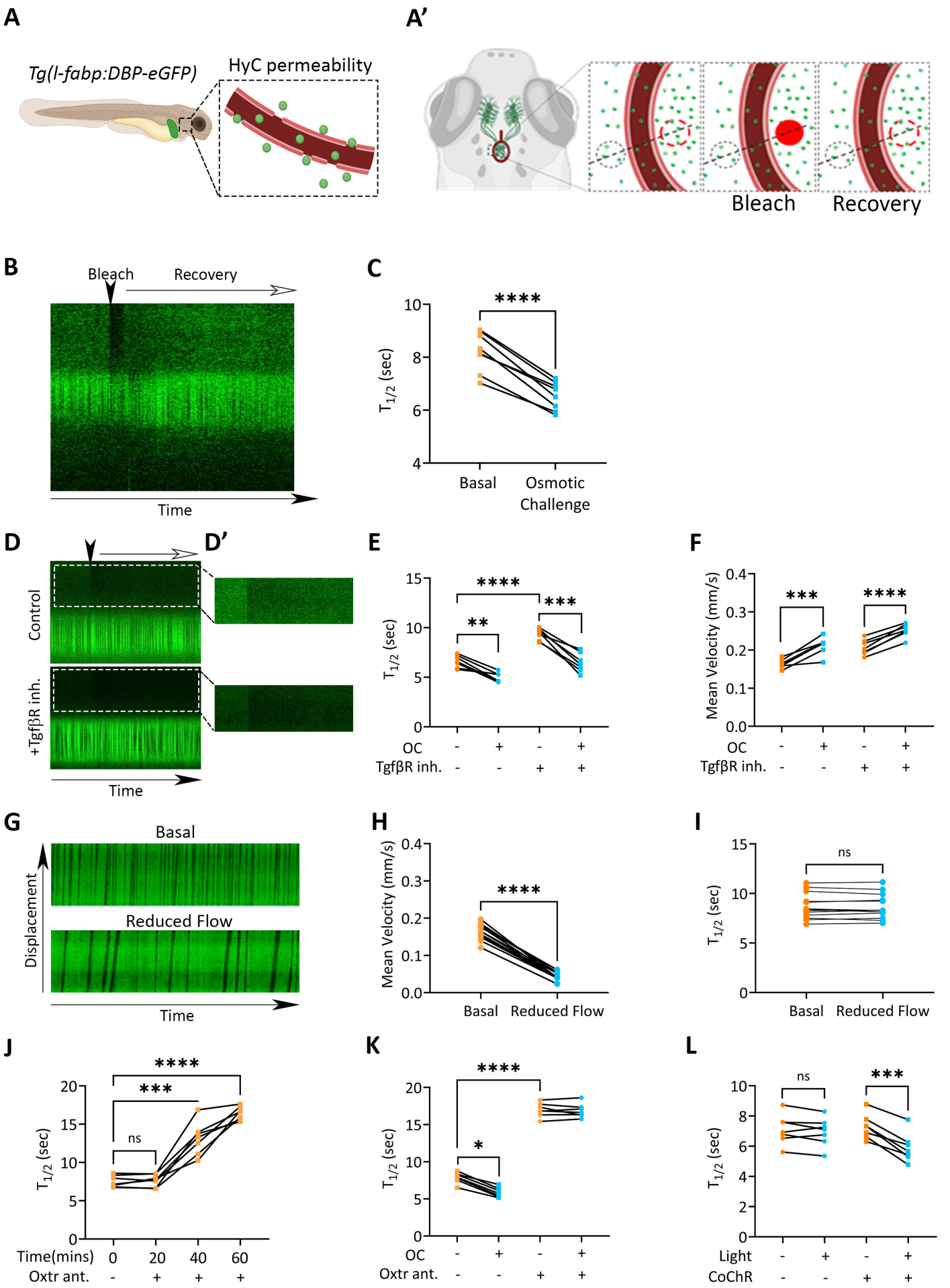
A
Tg(l-fabp:DBP-eGFP)
HyC permeability
A'
Bleach
Recovery
B
Bleach
Recovery
Time
C
****
$T_{1/2}$ (sec)
Basal
Osmotic Challenge
D
D'
Control
+TgfβR inh.
Time
E
****
***
**
$T_{1/2}$ (sec)
OC
TgfβR inh.
F
***
****
Mean Velocity (mm/s)
OC
TgfβR inh.
G
Basal
Reduced Flow
Displacement
Time
H
****
Mean Velocity (mm/s)
Basal
Reduced Flow
I
ns
$T_{1/2}$ (sec)
Basal
Reduced Flow
J
****
***
ns
$T_{1/2}$ (sec)
Time(mins)
Oxtr ant.
K
****
*
$T_{1/2}$ (sec)
OC
Oxtr ant.
L
ns
***
$T_{1/2}$ (sec)
Light
CoChR

Figure 6

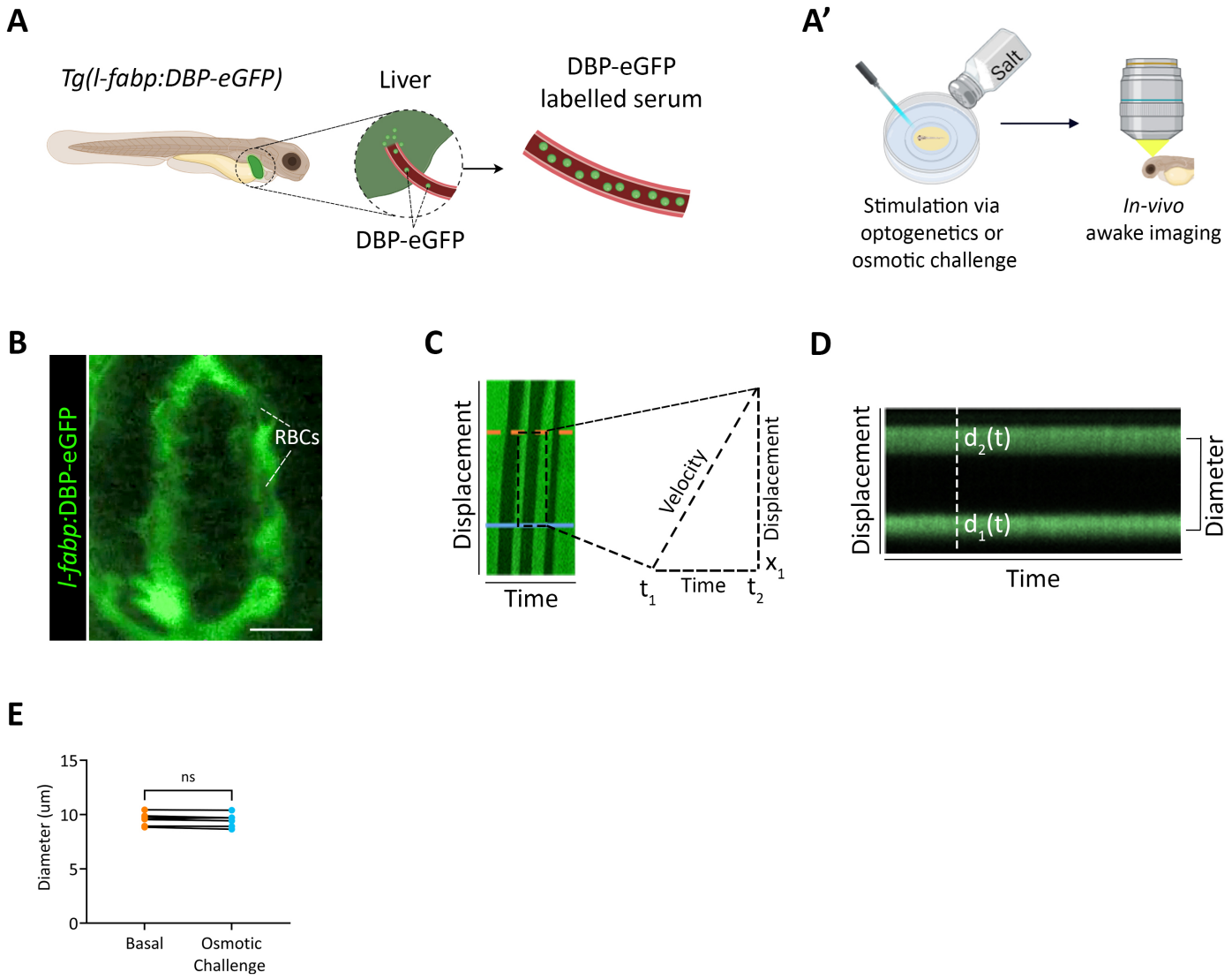

Supplement 1

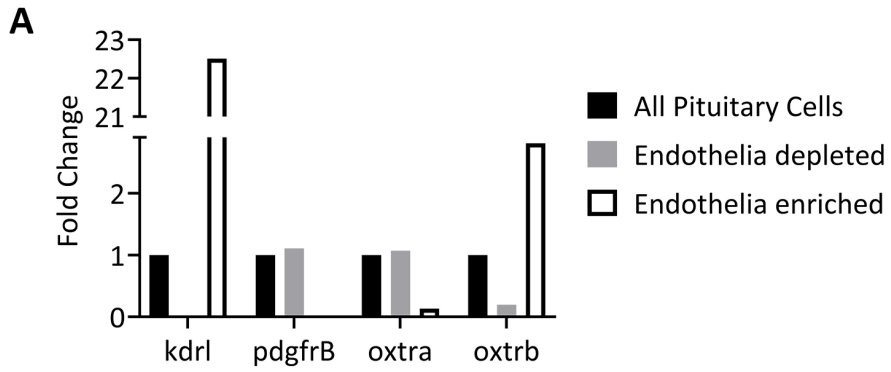

Supplement 2